Water Resources Research

RESEARCH ARTICLE
10.1029/2017WR022017

Modeling Subgrid Variability of Snow Depth Using the Fokker-Planck Equation Approach

Siwei He[1,2,3] **and Noriaki Ohara**[1]

[1]Department of Civil and Architectural Engineering, University of Wyoming, Laramie, WY, USA, [2]Now at National Research Council, Washington, DC, USA, [3]Now at NOAA/Earth System Research Laboratory, Boulder, CO, USA

Key Points:
- A physically based subgrid variability snow model using the Fokker-Planck equation (FPE) approach was proposed and validated
- Snow redistribution and snowmelt effects on the subgrid variability of snow depth were incorporated in the FPE snow model
- The FPE snow model can simulate the time evolution of probability density function of snow depth over a finite area

Supporting Information:
- Supporting Information S1

Correspondence to:
S. He,
she@uwyo.edu;
siwei.he@noaa.gov

Citation:
He, S., & Ohara, N. (2019). Modeling subgrid variability of snow depth using the Fokker-Planck equation approach. *Water Resources Research*, *55*, 3137–3155. https://doi.org/10.1029/2017WR022017

Received 5 OCT 2017
Accepted 13 MAR 2019
Accepted article online 21 MAR 2019
Published online 16 APR 2019

Abstract A physically based subgrid variability model for snow process using the Fokker-Planck equation (FPE) approach was proposed. This FPE can express the evolution of the probability density function (PDF) of snow depth within a finite area, possibly a grid cell of distributed models or a small basin, whose shape can be irregular. The main advantage of this approach is that it does not rely on a given PDF but dynamically computes the PDF through an advection-diffusion-type equation, the FPE, which was derived from point-scale process-based governing equations. Snow depth was treated as a random variable, while the snow redistribution and snowmelt rate were treated as the sources of stochasticity. The main challenge in solving this FPE is evaluating the time-space covariances appearing in the diffusion coefficient. In this study, approximations to evaluate the covariance terms, accounting for snowmelt and snow redistribution, were proposed. The simulated results of the FPE model were validated by the measured time series of snow depth at one site and the spatial distributions of snow depth measured by ground penetrating radar and airborne light detection and ranging (Lidar). It was shown that the point-observed snow depth fell within the simulated range during most of the 2-year study period. The simulated PDFs of snow depth within the study area were similar to the observed PDFs of snow depth by ground penetrating radar and Lidar. In summary, these results demonstrate the efficacy of the proposed FPE model representing the subgrid variability of snow depth.

1. Introduction

The spatial variability of snow depth is influenced by various factors, such as vegetation, topography, wind, and radiation. The spatial variability of snow depth can result in uncertainty in hydrological and atmospheric processes due to the presence of snow influencing the radiative and turbulent heat fluxes on the land surface (Essery, 1997; Liston, 1995; Luce et al., 1998; Menzel & Lang, 2005). Understanding snow spatial distribution is essential for quantifying it as a water resource and its effects on atmospheric circulation (He et al., 2019; Luce et al., 1998; Wetlaufer et al., 2016). In hydrological and land surface processes modeling, the total spatial variability can be treated as the sum of the small-scale variability within a computational cell and the large-scale variability between computational cells (Isaaks & Mohan Srivastava, 1989). The small-scale variability within a computational cell is also termed subgrid variability, while the large-scale variability between computational cells is also termed element-to-element variability (Blöschl, 1999). The element-to-element variability of snow depth is represented explicitly by distributed snow models, while most distributed snow models generally assume uniform snow depth within a computational cell and ignore the subgrid variability of snow depth. A higher spatial resolution model can better represent spatial variability, but the requirements for the forcing data and computational resources significantly increase. Generally, representing spatial variability in distributed models is a tradeoff between spatial resolution and model complexity (Liang et al., 1996).

There are two basic approaches for modeling the subgrid variability of snow depth or other hydrological variables (Liang et al., 1996; Yeh & Eltahir, 2005). One is the statistical dynamic approach (Avissar, 1992; Liang et al., 1996; Luce et al., 1999), and the other is the mosaic-based approach (Avissar, 1989; Seth & Giorgi, 1994). These two approaches can represent the subgrid variability for the majority of cases although they have some disadvantages. The statistical dynamic approach typically requires determining type of probability density function (PDF) before modeling, and the ensemble averaging technique in such a model often suffers from difficulty in evaluating the stochastic integral equation particularly for a nonlinear equation with large variations (e.g., Horne & Kavvas, 1997). The mosaic approach transfers the spatial variability

issue to an even smaller scale, which may never disappear. Modeling spatial variability of snow depth has been discussed based on empirical knowledge (e.g., Clark et al., 2011; Liston, 2004; Luce et al., 1999). In this paper, an alternative model to represent the dynamic subgrid variability of snow depth, which is formulated by a set of nonlinear equations, was proposed based on the Fokker-Planck equation (FPE) approach.

Kavvas (2003) derived a relationship between a general nonlinear hydrological conservation equation and a partial differential equation (PDE) in the probability domain. This PDE, known as FPE or backward Kolmogorov equation, is an advection-diffusion-type equation describing the evolving PDF. The variable that represents the state of the system is called state variable, and the source or sink term(s) is (are) called forcing variable(s). In the upscaled system representing a finite area, the state variable is called stochastic state variable, while the forcing variable(s) are called sources of stochasticity. Kavvas (2003) expanded point-scale conservation equations to corresponding stochastic partial differential equations by including heterogeneities of parameters and forcing variables to describe processes at a finite grid scale. These stochastic partial differential equations were then converted to FPE describing the evolving PDF of state variables. Under appropriate initial and boundary conditions, solutions of the FPE could be obtained. The approach to represent subgrid variability by solving the FPE is called the FPE approach in this article. Ohara et al. (2008) first used the FPE approach for modeling snow accumulation and melt processes in a finite area. They successfully demonstrated the potential of the FPE approach as a physically based parameterization of subgrid effects on the snow process for a short simulation period.

However, a few issues need to be resolved to make the FPE approach widely applicable. First, the FPE requires appropriate state variable selection to obtain a reasonable solution. Ohara et al. (2008) stated that one key step in using the FPE approach was to choose the right state variables and the external stochastic variables. Strictly speaking, all the state variable(s) are stochastic; however, the number of the state stochastic variables is basically equal to the number of the dimension(s) in the corresponding FPE. Thus, snow depth, which represented snow storage, was chosen as a state stochastic variable in this study for simplicity. Second, the sources of stochasticity in the FPE must be selected appropriately. The sources of stochasticity should be minimized without diminishing the reality of the model since sources of stochasticity appear as the cross-covariance terms that are often hard to evaluate. Snow depth is influenced by many factors, such as topography, precipitation, vegetation, wind, and snowmelt. The main influences were grouped into two terms, snow redistribution and snowmelt, and incorporated into the FPE in this study. Third, these sources of stochasticity, which appeared as time-space autocovariance terms in the FPE, must be quantified. These autocovariance terms were difficult to evaluate due to the limitations of the observed data and knowledge of the physical mechanisms of these processes. In this study, approximations to evaluate the covariance terms were proposed. Fourth, it is not straightforward to obtain a high accurate numerical solution because both convection and diffusion coefficients are time dependent with large variability. Thus, the simulated results of the FPE approach must be validated by the observed spatial distributions of snow depth in order to check the validities of the theoretical and numerical approximations introduced here.

The objective of this study is to test the FPE approach representing the subgrid variability of snow depth within a finite area (e.g., computational grid of distributed hydrological models or small watershed) for a season-long, continuous simulation. At the same time, this effort verifies the underlying assumption that Gaussian stochasticities of snow redistribution and snowmelt processes can effectively model the spatial variability of snow depth. The study proposes an effective alternative method for handling subgrid variability through demonstrating the effectiveness of the FPE model using the observed snow depth data.

This paper is presented in five sections: introduction, methods, model application, discussion, and conclusions. The derivation of the FPE of snow depth is presented in section 2, which includes explicit simplifications and the numerical method. In section 3, the proposed FPE approach is tested in the No-name watershed in southeastern Wyoming. Details on the evaluations of covariance terms are also included in this section. Lessons and conclusions drawn from this study are presented in sections 4 and 5.

2. Methods

2.1. Derivation of FPE

According to previous studies (Ohara & Kavvas, 2006), the point-scale governing equation for mass conservation of snow can be written in simultaneous ordinary differential equations as

$$\frac{dD}{dt} = \frac{\rho_w}{\rho_s}(-E - M_r + q + sn) - \frac{D}{\rho_s}\frac{d\rho_s}{dt} \tag{1a}$$

$$\frac{d\rho_s}{dt} = \frac{2}{3\eta}\rho_s D e^{0.04T_s - \mu\rho_s} - \frac{(\rho_s - \rho_{ns})\rho_w}{D\rho_{ns}} sn \tag{1b}$$

where D is the snow depth (m), t is the time (s), ρ_s is the average density of snowpack over depth (kg/m^3), ρ_w is the water density (kg/m^3), E is the sublimation rate (m/s), ρ_{ns} is the density of new snow (kg/m^3), M_r is the snowmelt rate (m/s), sn is the snowfall rate (m/s), q is the snow deposition or erosion rate by wind snow redistribution (m/s), T_s is the depth average snow temperature (°C), μ is a constant to be determined from the observed data (m^3/kg; Anderson, 1976; Kojima, 1967), and η is the empirical viscosity coefficient (m/s; Anderson, 1976; Kojima, 1967). In these equations, E, M_r, q, and sn are expressed in water equivalent units. Snowmelt, sublimation, and snow temperature at every time step are calculated based on energy balance (e.g., DeWalle & Rango, 2008). Each variable in equations (1a) and (1b) is a function of location within the grid since they are point-scale equations. By combing equations (1b) and (1a), the snow depth can be expressed as

$$\frac{dD}{dt} = F_t(\rho_s, E, M_r, q, \rho_{ns}, \eta, D, T_s, \mu, sn; \mathbf{x}, t), \tag{2}$$

where $\mathbf{x}$ is the space vector and t is the time. $\mathbf{x}$ and t appear because they are independent variables, while all other physical variables are dependent on $\mathbf{x}$ and t. F_t is a function that can be expressed as

$$F_t = \frac{\rho_w}{\rho_s}(-E - M_r + q) + \frac{\rho_w}{\rho_{ns}} sn - \frac{2}{3\eta} D^2 e^{0.04T_s - \mu\rho_s}. \tag{3}$$

According to Kavvas (2003) and Ohara et al. (2008), the corresponding FPE can be derived from equation (2) as

$$\begin{aligned}\frac{\partial P}{\partial t} = & -\frac{\partial}{\partial D}\left\{\left[\langle F_t\rangle + \int_0^t \mathrm{Cov}\left(F_{t-s}; \frac{\partial F_t}{\partial D}\right) ds\right]\cdot P\right\} \\ & + \frac{1}{2}\frac{\partial^2}{\partial D^2}\left\{\int_0^t \mathrm{Cov}(F_t; F_{t-s}) ds \cdot 2P\right\}.\end{aligned} \tag{4}$$

where P is the probability density of snow depth, $\langle\ \rangle$ is ensemble average operator, and Cov( ) is the time ordered covariance function (Kavvas & Karakas, 1996; van Kampen, 1976). This is the FPE for the spatially upscaled or integrated snow process modeling. The independent variables of this FPE are snow depth D and time t, and the solution is the probability density of snow depth $P(D,t)$. The dispersion term of the equation appears because of the second-order truncation of the formal cumulant expansion (Kavvas & Karakas, 1996; Kavvas & Wu, 2002). Equation (4) is in a form of convection-diffusion equation; however, it is not straightforward to obtain solutions due to the convection and diffusion coefficients, which include time-ordered covariance terms of the function F_t. With some simplifications (see supporting information), the FPE can be reduced to

$$\begin{aligned}\frac{\partial P}{\partial t} = & -\frac{\partial}{\partial D}\{\langle F_t\rangle P\} \\ & + \frac{\partial^2}{\partial D^2}\left\{P\left[\int_0^t \left(\frac{\rho_w}{\rho_s}\right)^2 \mathrm{Cov}(M_r(\mathbf{x}_t, t); M_r(\mathbf{x}_{t-s}, t-s)) ds + \int_0^t \left(\frac{\rho_w}{\rho_s}\right)^2 \mathrm{Cov}(q(\mathbf{x}_t, t); q(\mathbf{x}_{t-s}, t-s)) ds\right]\right\}.\end{aligned} \tag{5}$$

This is the simplified FPE, which describes time evolution of the probability density of snow depth with stochastic snow redistribution and snowmelt effects.

In the FPE approach, snow depth was treated as a stochastic state variable. There are two possibilities to describe the evolution of a stochastic variable using a mathematical model (Heinz, 2011). The first approach is an ensemble averaging with regular perturbation to quantify the uncertainty of state variable (e.g., Graham & McLaughlin, 1989; Horne & Kavvas, 1997; Wu et al., 2005; Zha et al., 2017), and the

second approach is the FPE and stochastic differential equation method to describe an evolution of the PDF of a stochastic variable (Kavvas, 2003; Yoon & Levent Kavvas, 2003; Kim et al., 2005; Ohara et al., 2008; Kure et al., 2010). This study belongs to the second approach. Both approaches require the ergodicity assumption that the spatial statistics over the grid or the finite area is equivalent to the ensemble statistics. This requires the area large enough to include all the possibilities in the ensemble. In other words, the ergodicity assumption ensures the FPE to be the upscaled governing equation for the grid or the finite area. Another assumption in the FPE approach is that the stochastic sources (M_r and q in this study) are Gaussian processes. Once these two conditions are met, solutions of the FPE can describe the evolution of the PDF of snow depth within a finite area (cf. a computational grid of a regional water balance model) without losing the physical properties of the process. Although the simulated mean can be calculated from the PDF, it is not necessary that one specific realization (i.e., point measurement) matches the mean. In principle, the mean should be matched by the average of many realizations (i.e., multiple point measurements).

2.2. Numerical Method for FPE

Equation (5) can be concisely written as

$$\frac{\partial P}{\partial t} = -\frac{\partial}{\partial D}\{\langle F_t\rangle P\} + \frac{\partial^2}{\partial D^2}\{(D_{iff}P)\} \tag{6}$$

where $\langle F_t\rangle$ is the convection coefficient and D_{iff} is the diffusion coefficient

$$\begin{aligned} D_{iff} &= \left(\frac{\rho_w}{\rho_s}\right)^2 \int_0^t \mathrm{Cov}(q(\mathbf{x}_t,t); q(\mathbf{x}_{t-s},t-s))ds \\ &+ \left(\frac{\rho_w}{\rho_s}\right)^2 \int_0^t \mathrm{Cov}(M_r(\mathbf{x}_t,t); M_r(\mathbf{x}_{t-s},t-s))ds. \end{aligned} \tag{7}$$

To ensure high accuracy in numerical solutions, a second-order numerical scheme is preferable for the FPE. This study adopted the Monotonic Upstream-centered Scheme for Conservation Laws (MUSCL) scheme to solve equation (6). The basic steps for implementing the MUSCL are given below (Hirsch, 2007).

The numerical fluxes J^* at the boundaries of the computational cell (from discretized snow depth) i can be expressed as the summation of fluxes in the negative and positive directions,

$$\begin{aligned} J^*_{i+1/2} &= J^+\left(\tilde{P}^{\mathrm{L}}_{i+1/2}\right) + J^-\left(\tilde{P}^{\mathrm{R}}_{i+1/2}\right), \\ J^*_{i-1/2} &= J^+\left(\tilde{P}^{\mathrm{L}}_{i-1/2}\right) + J^-\left(\tilde{P}^{\mathrm{R}}_{i-1/2}\right), \end{aligned} \tag{8}$$

where $J^*_{i+1/2}$ is the numerical flux of the right boundary at the computation cell i, $J^*_{i-1/2}$ is the numerical flux of the right boundary at the computation cell i, J is the function calculating flux and defined as

$$J = \langle F_t\rangle P. \tag{9}$$

Superscript + and − of J refer to the positive and negative $\langle F_t\rangle$. If $\langle F_t\rangle$ is positive, J^- terms disappear, and if $\langle F_t\rangle$ is negative, J^+ terms disappear. $\widetilde{P}$ is the modified probability density with the flux limiter Φ, superscript L and R refer to the left and right sides at the computational cell i, all $\widetilde{P}$ terms of equation (8) can be computed as

$$\begin{aligned} \tilde{P}^{\mathrm{L}}_{i+1/2} &= P_i + \frac{1}{2}\Phi^+_{i-\frac{1}{2}}(P_i - P_{i-1}), \qquad \tilde{P}^{\mathrm{R}}_{i+1/2} = P_{i+1} - \frac{1}{2}\Phi^-_{i+\frac{3}{2}}(P_{i+2} - P_{i+1}), \\ \tilde{P}^{\mathrm{L}}_{i-1/2} &= P_{i-1} + \frac{1}{2}\Phi^+_{i-\frac{3}{2}}(P_{i-1} - P_{i-2}), \qquad \tilde{P}^{\mathrm{R}}_{i-1/2} = P_i - \frac{1}{2}\Phi^-_{i+\frac{1}{2}}(P_{i+1} - P_i), \end{aligned} \tag{10}$$

and

$$\Phi^{+}_{i-1/2} = \Phi\left(r^{+}_{i-1/2}\right), \qquad \Phi^{-}_{i+1/2} = \Phi\left(r^{-}_{i+1/2}\right) \tag{11}$$

The ratio between successive gradients, r, can be estimated by

$$\begin{aligned} r^{+}_{i-1/2} &= \frac{P_{i+1}-P_i}{P_i-P_{i-1}}, \qquad r^{-}_{i+3/2} = \frac{P_i-P_{i+1}}{P_{i+1}-P_{i+2}}, \\ r^{+}_{i-3/2} &= \frac{P_i-P_{i-1}}{P_{i-1}-P_{i-2}}, \qquad r^{-}_{i+1/2} = \frac{P_{i-1}-P_i}{P_i-P_{i+1}}. \end{aligned} \tag{12}$$

For the diffusion term of equation (6), the central Euler method can be applied as follows:

$$\frac{\partial^2 P}{\partial D^2} = \frac{P_{i+1}-2P_i+P_{i-1}}{\Delta D^2} \tag{13}$$

Applying the forward Euler method for the time derivative term and combining the convection and the diffusion terms, equation (6) may be discretized as follows:

$$P^{n+1}_i = P^n_i - \frac{\Delta t}{\Delta D}\left(J^*_{i+1/2} - J^*_{i-1/2}\right) + \frac{\Delta t}{\Delta D^2} D^n_{iff}\left(P^n_{i+1} - 2P^n_i + P^n_{i-1}\right) \tag{14}$$

where n is the time index, Δt is the time step, and ΔD is the space step.

Through comparisons among the flux limiters, van Leer (van Leer, 1974), min-mod (Roe, 1986), superbee (Roe & Baines, 1982), and MUSCL limiter (van Leer, 1979), the MUSCL limiter showed the best performance for bell-shaped solutions. Thus, the MUSCL limiter was selected in this study. The MUSCL limiter (van Leer, 1979) can be expressed as

$$\Phi(r) = \max[0, \min(2r, (r+1)/2, 2)] \tag{15}$$

3. Model Application

3.1. Study Area

No-name watershed, which is a small subwatershed of the Little Laramie River Basin, is situated on the east slope of the Snowy Range in the Medicine Bow National Forest, Albany County, Wyoming (Figure 1). The elevations range from 2,920 to 3,060 m, and the catchment area is about 0.52 km^2. Vegetation is relatively uniform forest with spruce, lodgepole pine, and subalpine fir. The mean annual precipitation in the vicinity of the study area is about 900 mm, 50%–80% of which falls as snow between October and May (Holbrook, 2016). The annual mean air temperature is about 10 °C. This watershed has been implemented various surface and subsurface hydrological observation sensors supported by the Wyoming Center for Environmental Hydrology and Geophysics since 2012, making it is an ideal area to test the FPE model.

3.2. Data and Parameters

The red dot in Figure 1 shows the micrometeorological tower called *Repeater Tower*, which has meteorological sensors for air temperature (°C), relative humidity, wind speed (m/s), and precipitation rate (m/s). Since the precipitation gauge has some missing periods, the precipitation data of the Brooklyn Lake station, the SNOTEL station located nearby, were used as supplements. Brooklyn Lake station (41.3667°N, 106.2333°W, 3,121 m a.s.l.) is about 2.6 km to the northwest of the *Repeater Tower*. The meteorological data from the Glacier Lakes Ecosystem Experiments Site were also used as supplements for some data missing periods. The Glacier Lakes Ecosystem Experiments Site (41.3797°N, 106.3333°W, 3,286 m a.s.l.) operated by United State Forest Service is 5.2 km to the northwest of the *Repeater Tower*.

The model was validated using two types of snow depth data: time series and instantaneous spatial data. The time series data of snow depth were collected by a sonic sensor at the *Repeater Tower*. The spatial snow depth data were collected by ground-penetrating radar (GPR) and airborne light detection and ranging (Lidar). GPR provides rapid measurement of snow properties along a long transect (e.g., Marchand et al., 2003; Ulriksen & Peter, 1982). Several studies have shown that GPR is effective at imaging snow and glacier ice

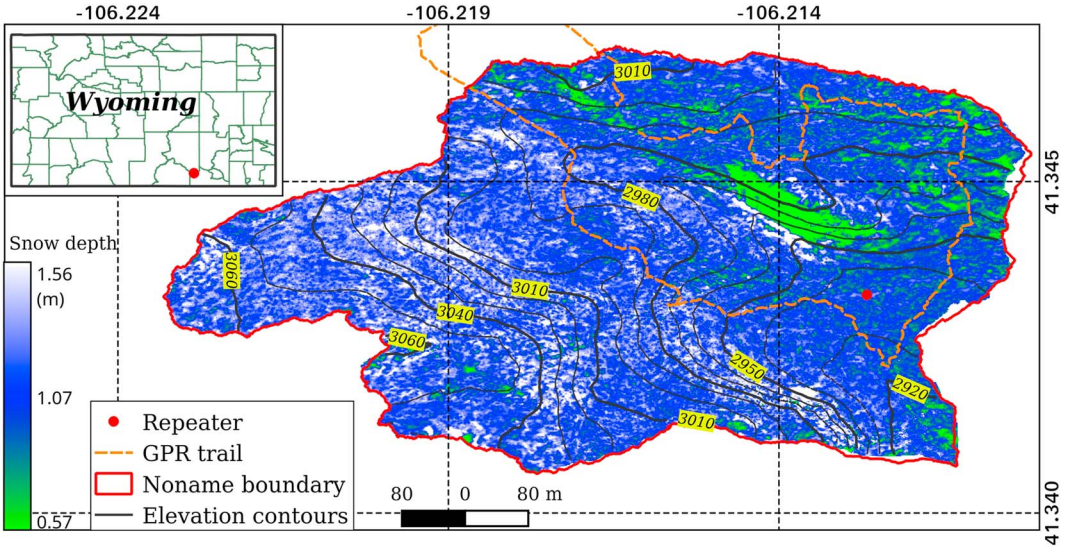

Figure 1. Location of the No-name watershed. The GPR trail and observed snow depths from Lidar are shown in this figure.

(Bradford et al., 2009; Holbrook, 2016; Marchand et al., 2003; Sundström, 2012). Lidar is a remote sensing tool with the ability to retrieve precision target positions at high spatial resolutions even in rough terrain and forested regions (Lefsky et al., 2002). Lidar-derived digital elevation models (DEMs) have accuracies as great as 10-cm root-mean-square error even in densely forested areas (Deems et al., 2013; Kraus & Pfeifer, 1998; Reutebuch et al., 2003). The airborne Lidar data with and without snow cover were used to derive an instantaneous spatial snow depth in the study area. In this study, the GPR data were collected on 11 April 2015, while Lidar data were collected on 16 April 2016. Based on the data quality and completeness, two snow seasons were selected for the model application. The first season was from 1 October 2014 to 20 June 2015, and the second from 1 October 2015 to 19 June 2016. The required physical and empirical parameters in the application are summarized in Table 1.

Since there was no snow accumulation in the study area on 1 October, the initial PDF of snow depth was expressed as a Dirac delta function at zero. The lower boundary is $D = 0$ as snow depth cannot be negative, and no flux boundary condition was used since the sum of probabilities should be conserved at one. The upper boundary should be a large number that snow depth cannot be reached, which is 3.0 m in this study.

Table 1
Notations, Physical Meaning of Parameters, and Their Values

Notations	Physical meaning	Values
dt	Time step (s)	3,600
ndt	Total time steps	6,500
dD	Snow depth step (m)	0.001
ρ_{ns}	New snow density (kg/m^3)	100
η	Viscosity coefficient, empirical (cm/hr)	21
μ	Viscosity coefficient, empirical (cm^3/g)	20
W_0	Water content of snow at 0 °C	0.05
t_c	Critical temperature for precipitation as snow (°C)	−1.0
f_{view}	View factor from snow surface to overhead forest	0.7
ε_f	Emissivity of forest canopy	0.93
ε_s	Emissivity of snow surface	0.98
κ_f	Extinction coefficient for shortwave in forest	0.32

3.3. Evaluation of Covariance

To solve the convection-diffusion equation (14), evaluation of the diffusion coefficient is required. From equation (7), the diffusion coefficient is expressed in terms of time-space covariance of snow redistribution rate q and snowmelt rate M_r. These two terms explicitly represent two major factors affecting the temporal and spatial variability of snow depth within a finite area such as a computational grid of a regional hydrological model, and these two covariance terms are dependent on time and space. If both covariance terms are kept as zeros throughout, then the resulting snow depth of the FPE model should be uniform within a finite area as in any deterministic snow model. In fact, the covariance terms are key components of the FPE approach representing the subgrid variability. However, due to the limitation of information, it is typically difficult to evaluate these time-space covariance terms for snow processes. When the correlation structures with respect to time, both in snow redistribution and snowmelt were ignored, equation (7) can be reduced to

$$D_{iff}(t) = \left(\frac{\rho_w}{\rho_s}\right)^2 \int_0^{\mathbf{x}} \mathrm{Cov}(q(\mathbf{x},t); q(\mathbf{x}-k,t))dk + \left(\frac{\rho_w}{\rho_s}\right)^2 \int_0^{\mathbf{x}} \mathrm{Cov}(M_r(\mathbf{x},t); M_r(\mathbf{x}-k,t))dk, \quad (16)$$

where k is spatial displacement. Although the delta correlation (uncorrelated white noise) with respect to time was assumed for both terms in this operation, the diffusion coefficient remains time dependent due to atmospheric forcing evolution. Proposed procedures for evaluating these two covariance terms will be discussed in the next.

3.3.1. Snow Redistribution

Snow redistribution can be caused by wind, vegetation, avalanche, and human activities. In this study, redistributions from wind and vegetation are considered.

Ohara (2014) showed that asymptotic snow distributions are often controlled by snow surface diffusion. In this case, snow redistribution, deposition/erosion rate due to wind (q_w) may be expressed as

$$q_w = \frac{1}{\rho_{ms}} \nabla \cdot (\mathbf{D}_{\mathrm{wind}} \nabla h), \quad (17)$$

where $\mathbf{D}_{\mathrm{wind}}$ is the diffusion coefficient tensor induced by wind turbulence (kg/m/s), h is snow surface elevation (m), ρ_{ms} is the density of mobile snow (kg/m^3), and ∇ is the Laplace operator in the two-dimensional Cartesian coordinate system (physical space) (x, y) [1/m]. It is important to distinguish this physical snow particle dispersion and the diffusion of the probability density function in the probability space. Equation (17) describes the curvature effect due to snow particle dispersion caused by snow surface erosion and deposition by acceleration and deceleration of wind around a topographic feature (Kimerling et al., 2012).

Numerous observational studies have demonstrated that vegetation (canopy) affects spatial variability of snow distribution over a scale of tens of meters (Broxton et al., 2015). However, there is no mathematical formulation that can be used to calculate this effect. Snowfall heterogeneity can be parameterized as a linear function of snowfall,

$$q_v = B \cdot sn \quad (18)$$

where B is an empirical coefficient that depends on the spatial variability of canopy and sn is snowfall rate (m/s). For example, uniform vegetation type corresponds to $B = 0$, while mixed forest and meadow land has a finite B value.

Accordingly, the covariance term of snow redistribution can be expressed as

$$\begin{aligned} \mathrm{Cov}\ (q(\mathbf{x},t); q(\mathbf{x}-k,t)) &= \mathrm{Cov}\left((q_w + q_v)\big|_{\mathbf{x},t}; (q_w + q_v)\big|_{\mathbf{x}-k,t}\right) \\ &= \mathrm{Cov}\left[\frac{1}{\rho_{ms}} \nabla \cdot (\mathbf{D}_{\mathrm{wind}} \nabla h)\Big|_{\mathbf{x},t}; \frac{1}{\rho_{ms}} \nabla \cdot (\mathbf{D}_{\mathrm{wind}} \nabla h)\Big|_{\mathbf{x}-k,t}\right] + \mathrm{Cov}\left[B \cdot sn\big|_{\mathbf{x},t}; B \cdot sn\big|_{\mathbf{x}-k,t}\right]. \end{aligned} \quad (19)$$

If the diffusion coefficient $\mathbf{D}_{\mathrm{wind}}$ is assumed to be isotropic and equals to D_{wind} and snowfall is spatially uniform within a finite grid size, equation (19) can be simplified as

$$\mathrm{Cov}(q(\mathbf{x},t); q(\mathbf{x}-k,t)) = \left(\frac{D_{\mathrm{wind}}}{\rho_{ms}}\right)^2 \mathrm{Cov}\left(\nabla^2 h\big|_{\mathbf{x},t}; \nabla^2 h\big|_{\mathbf{x}-k,t}\right) + \langle sn \rangle^2 \mathrm{Cov}\left(B\big|_{\mathbf{x},t}; B\big|_{\mathbf{x}-k,t}\right). \quad (20)$$

The snow surface diffusion coefficient D_{wind} was approximated by Ohara (2014) in terms of the turbulence component of wind as

$$D_{wind} \approx \frac{\rho_{cv}}{h_{cv}} k_*^2 \,\mathrm{var}(u_*) \quad (21)$$

where ρ_{cv} is density of snow within the control volume (kg/m^3), h_{cv} is thickness of the control volume (m), var(u_*) is the variance of friction wind speed (m^2/s^2), and k_* is the velocity-based snow drag coefficient.

Table 2
The Parameters and Their Values for Snow Redistribution Equations

Notations	Physical meaning	Values
h_{cv1}	The thickness of control volume during snowfall (m)	4.31
h_{cv2}	The thickness of control volume during blowing snow (m)	0.09
ρ_{bs}	Density of blowing snow (kg/m^3)	1.0
k'_{drag1}	Empirical snow drag coefficient during snowfall ($sn > 0$) (kg/m^2)	3.0
k'_{drag2}	Empirical snow drag coefficient during blowing snow ($u_* > u_{*c}$) (kg/m^2)	0.025
u_{*c}	Critical friction wind speed for snow movement (m/s)	0.4

Thickness of the control volume is the atmospheric layer where snow particle mixing takes place. The snow drag coefficient represents the proportionality between wind speed and snow particle velocity. Ohara (2014) related the snow drag coefficient to the empirical drag coefficient, as follows:

$$k_* = \begin{cases} \frac{1}{\rho_{bs} h_{cv1}} k'_{drag1} & \text{when } sn>0 \\ \frac{1}{\rho_{bs} h_{cv2}} k'_{drag2} & \text{when } u_*>u_{*c} \\ 0 & \text{otherwise} \end{cases} \quad (22)$$

where ρ_{bs} is the density of blowing snow (kg/m^3), k'_{drag} is the empirical snow particle drag coefficient (kg/m^2), and u_{*c} is the critical friction wind speed (Ohara, 2014). The surface diffusion coefficient of equation (21) represents wind-caused snow redistribution occurring during snowfall and subsequent snow accumulation. However, parameter h_{cv} and k'_{drag} can be different for different conditions (Ohara, 2014). The values of these parameters adopted in this study are shown in Table 2.

For wind-caused snow redistribution during snow transport or a blowing snow event, critical wind speed should be considered since any particle movement must first overcome the critical shear stress (e.g., He & Ohara, 2017). However, during snowfall, the thickness of control volume h_{cv} and drag coefficient k'_{drag} must be larger than the blowing snow case since snow particles must be in the air above the tree tops. These parameters were estimated from the typical surface layer thickness (bottom 10% of atmospheric boundary layer, e.g., Stull, 1988) and the upper limit of the drag coefficient estimates (Ohara, 2014).

Equation (21) illustrates that the variance of wind speed is essential for evaluating the snow surface diffusion coefficient. However, the meteorological data do not include the variance of wind speed. Based on the relationship between standard deviation and the friction velocity of wind speed in the atmosphere boundary layer, estimation of the variance of wind speed from the given mean wind speed can be derived as

$$\mathrm{var}(u_*) = m \cdot \langle u \rangle^2, \quad (23)$$

where m is the coefficient and $\langle u \rangle$ is the mean wind speed. Details on the derivation of this equation can be found in the Appendix A.

An eddy covariance sensor can be used to determine the coefficient m in equation (23). In this study, high-frequency (10-Hz) data from an eddy covariance tower in the No-name watershed (41.3438°N, 106.2124°W, 2,770 m a.s.l.) was used to estimate the coefficient m. The mean and variance of wind speeds were computed from a 1-hr moving window. The calculated means and variances from the eddy covariance tower high-frequency (10-Hz) data during the study period are plotted in Figure 2. Figure 2 shows that variances and means have a good linear relationship after removing outliers. According to the fitting result, $m = 0.261$.

Equation (20) indicates that the covariance of snow redistribution is proportional to the spatial covariance of the subgrid surface curvature $\nabla^2 h$. Therefore, the elevations of snow surface within the area of interest are required. Here we propose that the curvature of the snow surface can be approximated by the curvature of ground surface. This assumption may be reasonable especially in mountainous areas where the magnitude of topography variation is much larger than snow depth. The curvature is calculated using the method

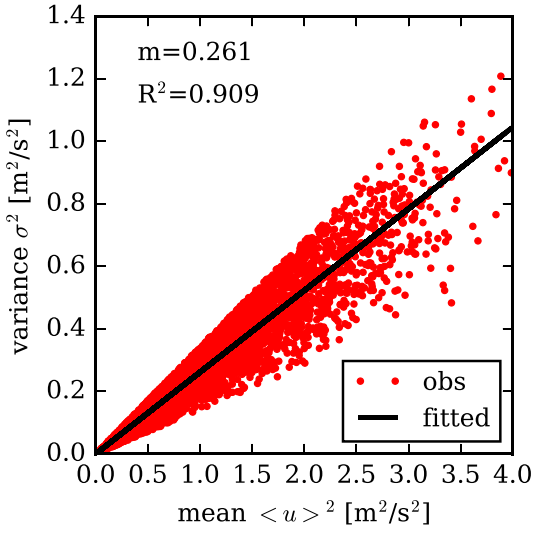

Figure 2. Scatter diagram of means and variances of the high-frequency data from eddy covariance tower in the No-name watershed.

suggested by Zevenbergen and Thorne (1987). In this study, Lidar-observed DEM (digital elevation model) data at 3-m resolution were used to calculate curvatures.

To integrate the covariance of curvature, it is necessary to calculate the spatial autocorrelation function (ACF) of curvature. The sample spatial autocorrelation function can be calculated by

$$g(k) = \frac{\sum_{i=1}^{n}\left(M(\mathbf{x})-\bar{M}\right)\left(M(\mathbf{x}-k)-\bar{M}\right)}{\sqrt{\sum_{i=1}^{n}\left(M(\mathbf{x})-\bar{M}\right)^2\sum_{i=1}^{n}\left(M(\mathbf{x}-k)-\bar{M}\right)^2}} \tag{24}$$

where $g(k)$ is the spatial autocorrelation coefficient, M is the variable (in this case, $\nabla^2 h$), k is the spatial displacement (lag), and n is the number of pairs at certain distance lag k. Figure 3 shows the computed sample spatial autocorrelation function of the surface curvatures for the No-name watershed.

Figure 3 shows that the spatial correlation of the topographic curvature has short memory. Because the spatial *memory* diminishes within 25 m, which is much smaller than the watershed size, the delta correlation approximation may be valid. Accordingly, the covariance of curvature of surface elevation can be simplified as

$$\mathrm{Cov}\left(\nabla^2 h(\mathbf{x},t);\nabla^2 h(\mathbf{x}-k,t)\right)\approx\mathrm{Cov}\left(\nabla^2 z(\mathbf{x},t);\nabla^2 z(\mathbf{x}-k,t)\right)\approx\mathrm{var}\left(\nabla^2 z(\mathbf{x})\right) \tag{25}$$

where z is the ground surface elevation. The first approximation in this equation is valid when the curvatures of subgrid snow surface do not differ from the curvatures of subgrid ground surface. The second approximation in equation (25) is valid when the delta correlation can be reasonably assumed for the spatial correlation of the subgrid surface curvatures.

The practical assumptions and approximations were introduced for the first term of the diffusion coefficient in equation (6). Table 3 lists the values for application of the model in the No-name watershed.

3.3.2. Snowmelt

Spatial variability of snowmelt or surface energy balance is influenced by solar radiation, albedo, topography, vegetation, and ground thermal properties. Since it is difficult to measure snowmelt rate distributions efficiently within the study area, a distributed snow model was used to estimate the spatial-temporal variability of snowmelt rate in this study. The covariance of snowmelt rate was calculated and analyzed using the simulated snowmelt rate.

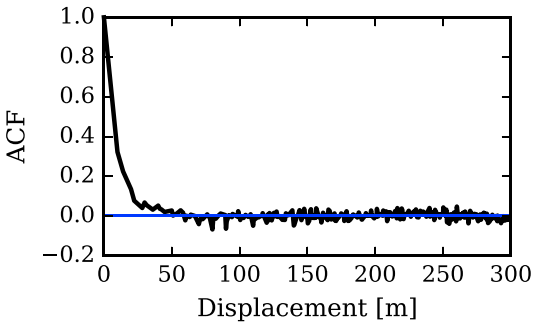

Figure 3. The autocorrelation coefficients of curvatures of No-name watershed. The curvatures are calculated from a 3-m DEM.

The distributed snow model (Dsnow; Ohara & Kavvas, 2006) is a distributed energy balance snowmelt model. The Dsnow input data are DEM data, aspect, slope, vegetation, and meteorological data (precipitation, humidity, wind speed, longwave radiation, shortwave radiation, and air temperature). The input meteorological data were obtained from the dynamically downscaled NCEP/NCAR Reanalysis Project (NNRP) data using the Weather Research Forecast model verified by field observations (Heward, 2015). In this study, the spatial resolution of the Dsnow model was 30 m and the time step was 1 hr. Detailed documentation on the configuration of the Dsnow model and validation of the results are recorded in Heward (2015). The ACF for snowmelt rate is calculated by equation (24) using the simulated snowmelt rate. Figure 4 shows the computed hourly sample spatial autocorrelation coefficients of snowmelt rate at different times and dates over the No-name watershed. In Figure 4, the left panel shows the spatial autocorrelation coefficients of snowmelt rate at different hours on 17 March, and the right panel displays those on 17

Table 3
The Parameters and Their Values for Calculating the Covariance of Snow Redistribution

Notations	Physical meaning	Values
ρ_{ms}	Density of mobile snow (kg/m^3)	80
ρ_{cv}	Snow density within the control volume (kg/m^3)	80
m	Proportionality coefficient of mean and variance of wind speed	0.261
var($\nabla^2 z$)	Variance of topography spatial curvature (m^{-2})	2.33E−3

June. Different lines represent different local times during the day. When the snow had melted at only a small number of grids, the autocorrelation function could not be reasonably computed. This figure clearly shows that the snowmelt happened only partially on 17 March, while on 17 June substantial snowmelt had occurred. The graphs indicated that the spatial ACFs of snowmelt rate have long correlation length or long memory. The strong spatial autocorrelation of the snowmelt rate in the study area makes the calculation of covariance of snowmelt difficult.

Because apparent long memory properties are often due to trend or cluster structure in the data, removal of the local mean values from the original data is necessary. Moreover, recalling the FPE (equation (6)), the effect of mean snowmelt rate has already been accounted for in the advection term and does not contribute to the diffusion term. Thus, it is appropriate to remove the local mean of snowmelt rate before evaluation of the diffusion coefficient. Figure 5 shows the spatial correlation coefficients of snowmelt rates during the two selected days after subtraction of moving window average (window size = 300 m). Although subtraction of the moving average effectively reduces the large-scale correlation (or long memory structure) from the original ACFs (Figure 4), a long tail (~150 m) still remains in the ACFs in Figure 5 compared to the window size (300 m). Hence, the delta correlation assumption may be inappropriate. However, the spatial ACFs of snowmelt rate converge to a single line even at different times of day and on different days of the year. This means that we can separate the time-dependent variance component from the stationary ACF as

$$\mathrm{Cov}(M_r(\mathbf{x}_t,t);M_r(\mathbf{x}_{t-s},t)) = \mathrm{Var}(M_r(\mathbf{x},t))g(k) \tag{26}$$

where $g(k)$ is the spatial ACF that was estimated from the sample by equation (24). Then, the ACF of snowmelt rate can be approximated by an exponential function,

$$\hat{g}(k) = \exp(-k/A) \tag{27}$$

where A is the fitted correlation length, $\hat{g}(k)$ is the fitted spatial ACF. The fitted lines are shown in Figure 5. To evaluate the diffusion coefficient in the FPE, equation (27) is substituted into equation (26) and then integrated over a certain range. The range of the integration is typically three times the correlation length, A (Western et al., 1998). Therefore, we have

$$\int_0^{3A}\mathrm{Cov}(M_r(\mathbf{x},t);M_r(\mathbf{x}-k,t))dk \approx \mathrm{Var}(M_r(\mathbf{x},t))\int_0^{3A}\hat{g}(k)dk = \mathrm{Var}(M_r(\mathbf{x},t))0.95A \tag{28}$$

This equation indicates that the covariance term can be evaluated from the known variance of snowmelt. The sample variance and mean of snowmelt rate were calculated, as shown in Figure 6.

It was found in Figure 6 that (1) the variance of snowmelt peaked around 14:00 every day when mean snowmelt rate typically was maximum; (2) the variance of snowmelt rate is zero as mean snowmelt rate is

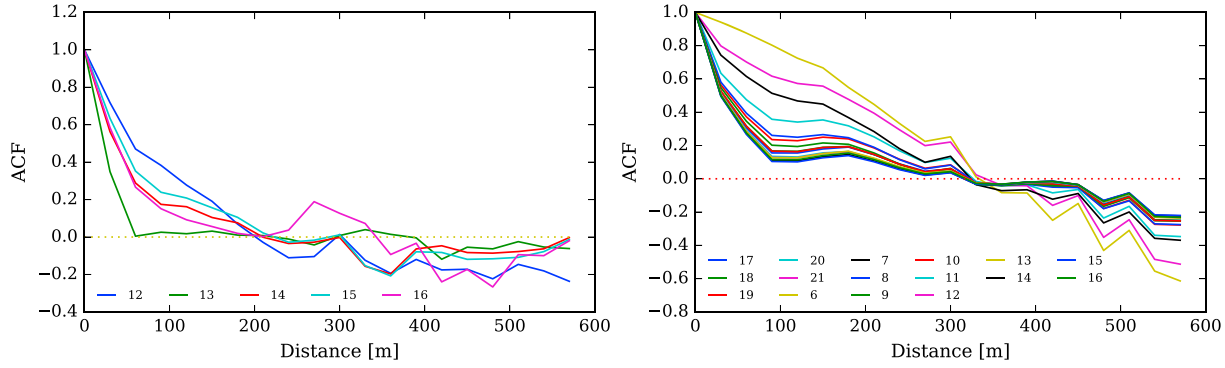

Figure 4. Hourly spatial autocorrelation coefficients of snowmelt rate at different dates and times (different lines represent different times, which are given in the legend). The left one for 17 March 2014 and the right one for 1 June 2014 (Mountain Time).

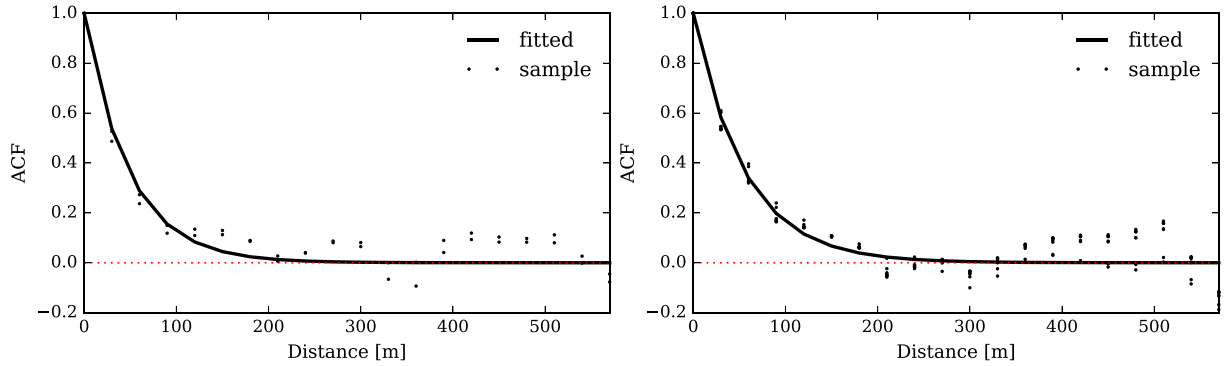

Figure 5. Hourly spatial autocorrelation coefficients of snowmelt rate at different dates and times after subtracting the moving averages. The fitted exponential models for the ACFs are superimposed as well. The left one for 17 March 2014 and the right one for 17 June 2014.

zero; and (3) both variance and mean of snowmelt have diurnal cycles. Accordingly, it may be feasible to estimate the variance of snowmelt rate from the mean values. Figure 7 shows the scatter diagram of the Dsnow-simulated mean and standard deviation of snowmelt rate over the No-name watershed from March to June 2014. Although further research is required for transferability, a correlation between the mean snowmelt rate $\langle M_r \rangle$ and the standard deviation of snowmelt rate $\mathrm{Std}(M_r)$ is evidentin this watershed. This relationship can be fitted by an exponential function as Figure 7 is on *log-log* plane. That is

$$\log(\mathrm{Std}(M_r)) = b + a\ \log(\langle M_r \rangle), \tag{29}$$

where a and b are the slope and intercept in *log-log* plane. The fitting parameters were found to be $a = 0.53$ and $b = -9.35$ with $R^2 = 0.85$ for the No-name watershed from the distributed snow model outputs. For the

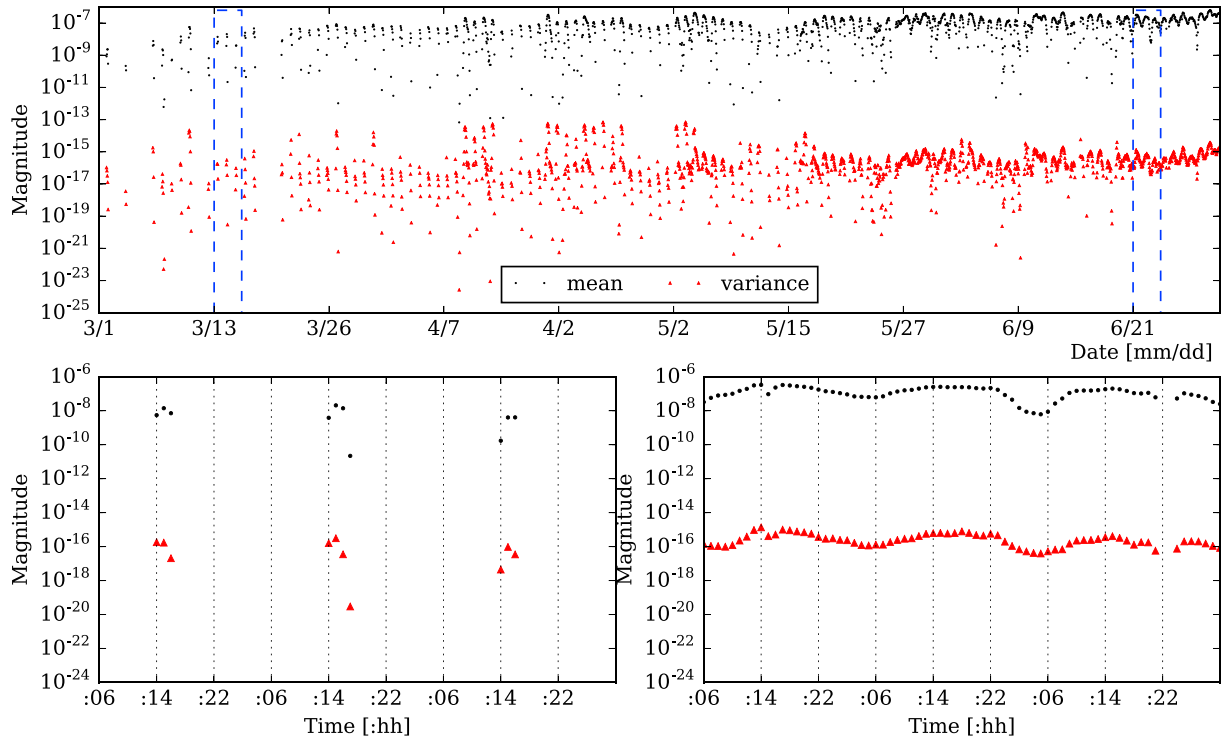

Figure 6. Variance and mean of hourly snowmelt changes with time (year 2014). The two subfigures at the bottom are zoomed-in on the periods with dashed rectangles.

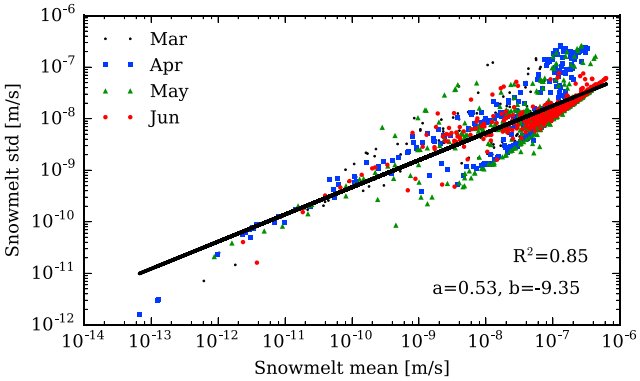

Figure 7. Relationship between the mean value and standard deviation of snowmelt. The Dsnow- modeled hourly snowmelt rate for the year 2014 from March to June are used.

simulation, the variance of snowmelt was evaluated from standard deviation that obtained using this relationship. However, applicability of this empirical relationship for other areas needs to be further researched.

In summary, the diffusion coefficient of the FPE, equation (16), was evaluated by

$$D_{iff}(t)=\left(\frac{\rho_w}{\rho_s}\right)^2\left[m\left(\frac{\rho_{cv}k_*^2}{\rho_{ms}h_{cv}}\right)^2\mathrm{var}\left(\nabla^2 z(\mathbf{x})\right)\langle u\rangle^2+\langle sn\rangle^2\beta+0.95A\cdot e^b\langle M_r\rangle^a\right] \tag{30}$$

where β is the empirical coefficient in the forest canopy parameterization ($\beta = \int \mathrm{Cov}(B|_{\mathbf{x}};\ B|_{\mathbf{x}\ -\ k})dk$). The diffusion coefficient in this model (equation (30)) was mainly influenced by three variables: wind speed, vegetation distribution, and snowmelt rate. All model parameters except β were determined through the above described process-based methodology. However, the parameter β was determined to be 1,500 by a trial-and-error calibration procedure for the snow depth time series and for the instantaneous probability density function of snow depth. All unknown effects on snow distribution (cf. uneven sublimation) must be absorbed by this second term in equation (30). This residual effect, which was called *vegetation effect* in this article, will be discussed in section 3.4. The parameters and their values for calculating the covariance of snowmelt are given in Table 4.

3.4. Results

The time series of the simulated snow depth and the observed snow depth are compared in Figure 8. The 95% confidence interval (CI) of the simulated snow depth is denoted by the shaded area. With the FPE approach, the standard deviation of snow depth can be easily computed from the simulated PDF. This CI is an important output of the FPE model since it is generally difficult to estimate variance using deterministic models. The CI shows that the spatial variability of snow depth increases as time increases. The observed snow depth data at the *Repeater Tower* are shown in blue colored dots in Figure 8. The observed snow depths, which likely represent the mean values in the watershed, are fairly close to the mean snow depths within the CI, although there are some discrepancies. Figure 8 also shows vertical lines indicating snow depth survey dates using GPR and airborne Lidar over the study area on 11 April 2015 and 16 April 2016.

The simulated PDFs of snow depth at different times are presented in Figure 9 illustrating the evolution of spatial snow distribution in the watershed. The PDF of snow depth moves to the left with snowmelt and to the right with new snowfall. Also, the PDF diffuses with time due to snow redistribution and uneven snowmelt effects. Moreover, some of these evolving PDFs cannot be well fitted by any common distributions, such as uniform, normal, lognormal, or Gamma distributions. This suggests that it is inappropriate to use one specific PDF for an entire snow season.

The spatial distributions of snow depth in the No-name watershed were measured using the GPR on 11 April 2015 and the airborne Lidar on 16 April 2016, as shown in Figure 10. The filtered PDFs, histograms, and PDFs of the simulated snow depths are shown in Figure 10. The filtered PDF was derived from the measurements to visualize the true PDF of a random variable (Heinz, 2011). If the sample size is large enough, the filtered PDF can be treated as the true PDF. This figure demonstrates that the distributions of the simulated and measured snow depth are comparable. However, there are some differences between the PDF measured by GPR and the simulated PDF of snow depth because the GPR trails only cover a valley part of the study area as shown in Figure 1. Therefore, the observed PDF measured by GPR is biased. For the Lidar data that were collected on 16 April 2016, the resolution is 0.5 m and there are enough data (>10^8 samples) that cover the entire study area to calculate the filtered PDF. Therefore, the PDF estimated by the Lidar data is more representative. There is only a 3-cm difference in the

Table 4
The Parameters and Their Values for Calculating the Covariance of Snowmelt

Notations	Physical meaning	Values
A	Fitted correlation length (m)	50
a	Empirical fitting coefficient	0.53
b	Empirical fitting coefficient	−9.35

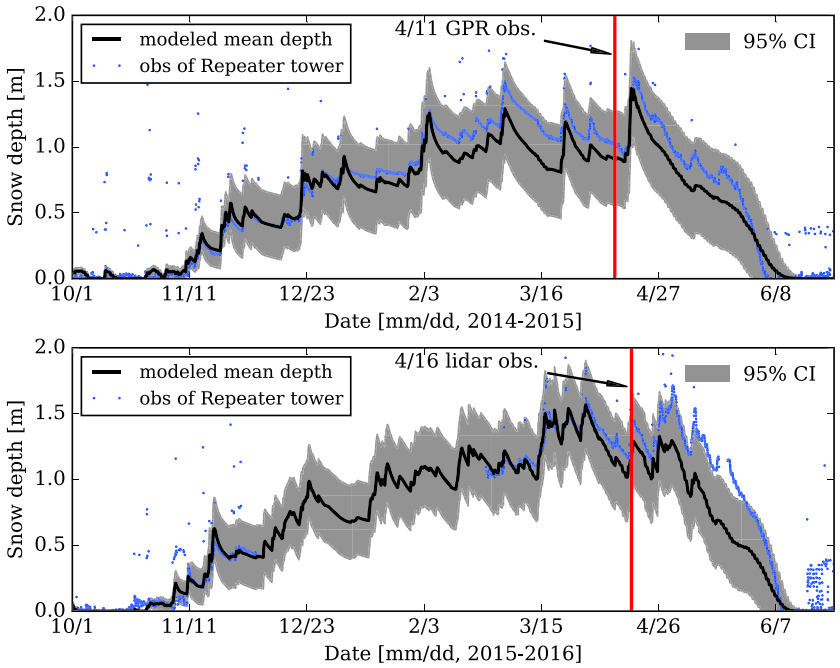

Figure 8. Comparison of simulated and observed snow depth. Points represent the observed snow depth from *Repeater Tower*. Solid line represents the simulated mean snow depth, gray shade is the simulated 95% confidence interval of the FPE snow model, and the vertical line is the date of spatial snow depth survey.

watershed average snow depth between the modeled and the Lidar-observed values. The spatial distribution of snow depth was represented reasonably well even with several approximations and simplifications. The statistical requirements (law of large numbers and ergodicity) for the theory were met even for this small watershed (0.52 km^2) as the ensemble average equation could generally describe

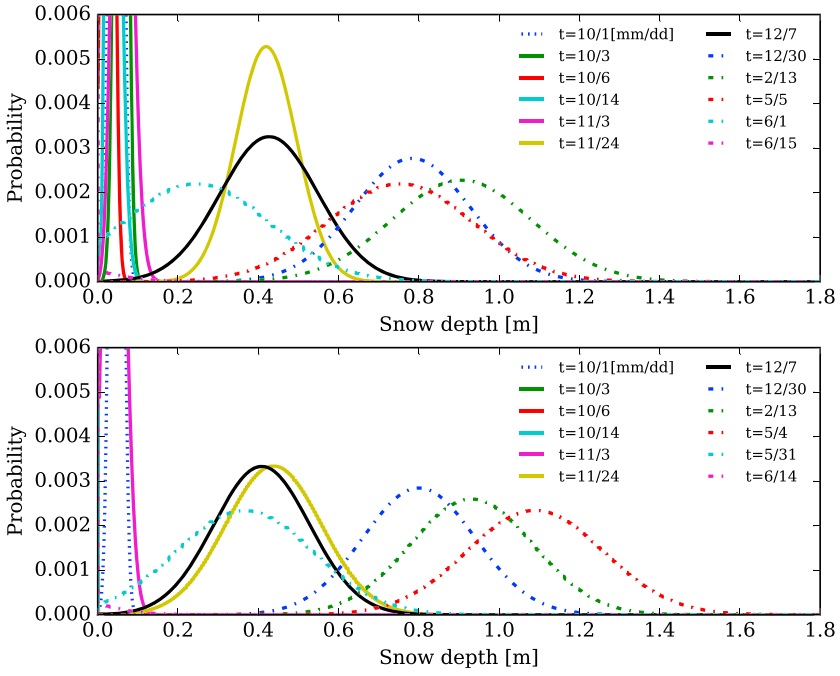

Figure 9. Evolution of PDF with time. The top panel is for snow season 2014–2015, while the bottom one is for snow season 2015–2016. Different lines represent different times.

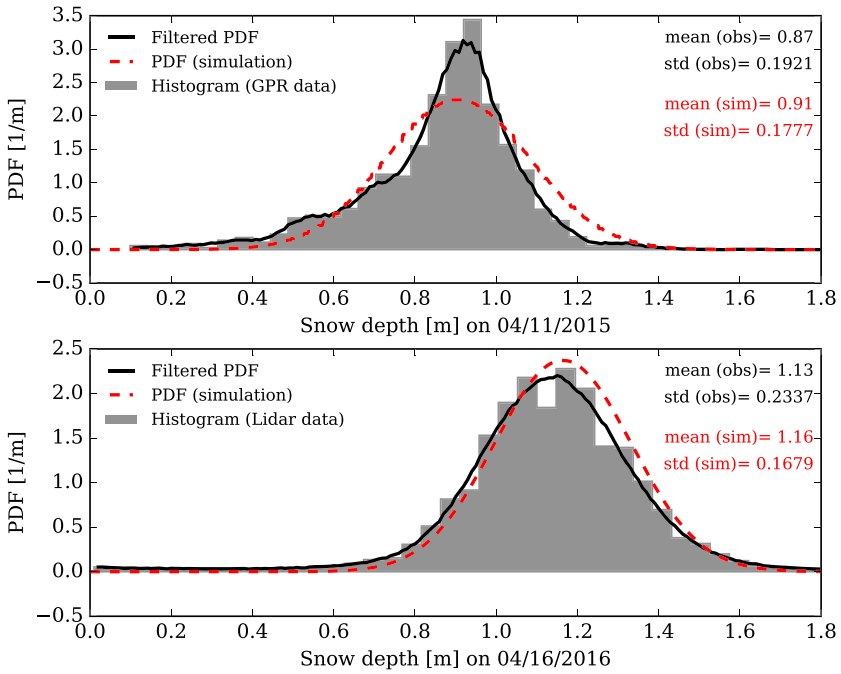

Figure 10. The simulated and observed spatial variability of snow depth. The dashed line is the simulated PDF, and the solid line is the filtered PDF from measurement data.

the real snow depth PDF and one-time series realization. Consequently, the carefully configured FPE model was able to reproduce the snow distribution in a finite area.

The diffusion coefficient in the FPE model has three components: wind-caused redistribution, uneven snowmelt, and from other redistributions (e.g., vegetation effects). These three components of the diffusion coefficient are shown in Figure 11. From these results, it was found that the dominant component of diffusion

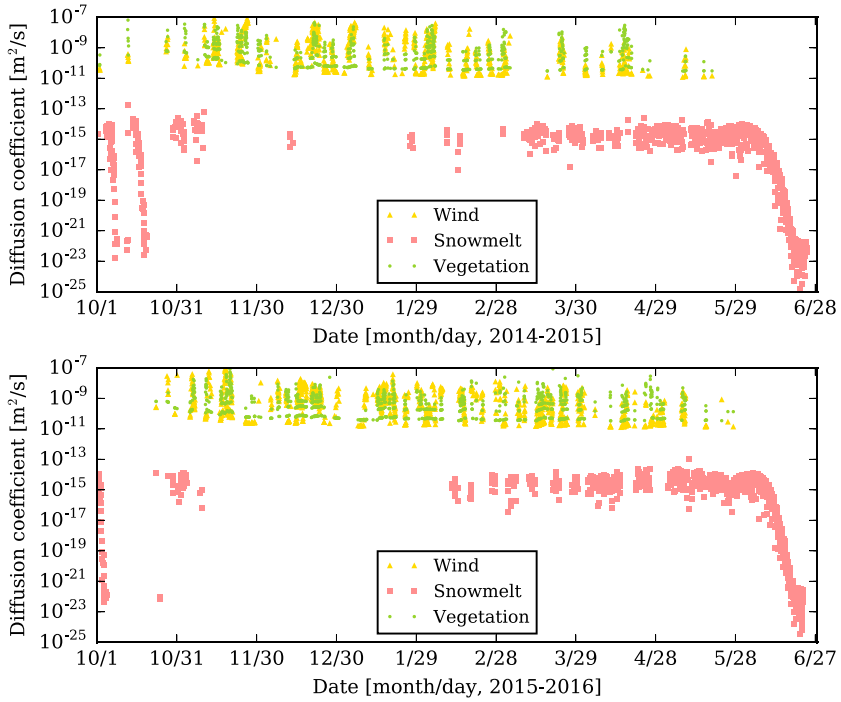

Figure 11. Computed components of diffusion coefficient during the simulated period.

coefficient is snow redistribution, which is caused by vegetation and wind in this study area. The effects of snowmelt on the spatial variability were more continuous, but much smaller by 2 orders of magnitude than the redistribution effects.

The total seasonal contributions of wind, vegetation, and snowmelt components to the spatial variability of snow depth were 65.5%, 34.5%, and 0.0%, respectively, in the 2014–2015 season and 62.9%, 37.1%, and 0.0%, respectively, in the 2015–2016 season. This suggests that more than 60% of snow redistribution in the forested study area was caused by wind. These findings are consistent with other studies showing that redistribution factors were more important than the snowmelt factors in determining the spatial variability of snow depth (Anderton et al., 2004; Dunn & Colohan, 1999; Hartman et al., 1999; Luce et al., 1998).

4. Discussion

Factors contributing to the snow depth variability may depend on the landscape and the size of the study area. For example, snow redistribution in an open area requires additional parametrization for the downwind snowdrift effect and the snow particle dispersion because the snow distribution downwind of an object is typically influenced by snow drift and eddy effects (e.g., Ohara, 2017). Mixed forest may result in larger snow diffusion than seen in this small No-name watershed covered by relatively uniform forest (e.g., He et al., 2019). If the diffusion coefficient in the FPE can be reasonably estimated, complicated snowdrift process modeling may be avoided. For a large area, the orographic effect of snow precipitation must be considered because uniform precipitation cannot be assumed. For example, if this FPE model is coupled with a regional- or global-scale model, the effect of the orographic precipitation within a model cell can be significant. At the same time, it is important to keep in mind that the size of the study area must be large enough to ensure meeting theoretical conditions such as the law of large numbers and ergodicity.

The snowmelt effect on the snow depth variability in the No-name watershed was small probably due to the study area uniformity. Because the Lidar data were collected during the peak snow season (He et al., 2019), before the start of the snowmelt season, verification of the snowmelt effect was inconclusive in terms of the PDF. It is possible that the distributed snow model (Dsnow), which was used to determine the snowmelt variance, may overestimate the energy flux suppression by the forest canopy. Quantification of spatial variety in energy balance is challenging in a forested area. For open terrain, the snowmelt effect may be more pronounced than in the No-name watershed study area. Thus, the proposed FPE model still requires careful consideration in model parameterizations and parameter estimations for other applications.

This study resolved the issue of numerical instability for the FPE in the use of this model. This new algorithm with single-variated FPE described snow development and disappearance periods when the land surface was partially covered by snow. These periods are particularly difficult as the PDF near the lower boundary (i.e., $D = 0$) often becomes very steep or approaches discontinuity. The numerical scheme presented in section 2.2 was robust enough to manage the mathematical instability. In representing subgrid variability of snow over a certain domain, the number of required parameters for the FPE model is fewer than for the distributed snow model, although several of the stochastic parameterizations are not available. Also, the FPE model has the potential to save computational resources because the spatial interpolation of the model parameters and atmospheric forcing is less intensive.

More data collection of snow distribution at fine spatial and temporal resolutions is desirable for further model development and validation. Obviously, there is room for improvement in model validation; existing observation data does not allow partitioning the effects acting on snow distribution. As such, it is reasonable to limit the number of state variables to one and the number of stochasticity sources to two, in order to focus on snow mass exchange. It is likely acceptable to assume that snowmelt and snow distribution are independent of each other and are very different processes: energy balance versus snow dynamics. The snowmelt process is typically controlled by surface energy balance, while the snow redistribution process is mainly induced by the surface wind field. We introduced an additional term, vegetation-related redistribution, which acts as a closure term in the current version. It is possible that this version misses

one or more important effects, such as the downwind snowdrift effect. However, this modeling effort points to the direction in which snow modeling can progress and what data types are needed for upscaled snow modeling.

5. Conclusions

The concept of a FPE model representing the subgrid variability of snow depth was tested using observed spatial distribution and time series snow depth data. Although FPE model development was initiated by Ohara (2003) and Ohara et al. (2008), they struggled to manage bivariate FPE (two stochastic state variables) for long-term simulations (cf. more than 3 days). In this study, the FPE was simplified further by reducing it to one stochastic state variable, while significant additional model components for the source heterogeneities were introduced. The results showed that this new model successfully simulated the evolution of spatial distribution of snow depth. This upscaled snow model can be coupled with a regional- or global-scale land surface model (e.g., a few to several kilometers spatial resolution) because the FPE describes the PDF evolution of snow depth in a finite area. This new snow model may be the first season-long continuous model based on the FPE approach, which can explicitly represent the subgrid variability and possibly uncertainty of snow depth.

Two sources of stochasticity, snow redistribution and uneven snowmelt, were incorporated in the FPE model. The FPE was solved using a second-order numerical scheme, MUSCL, and it was applied to a small watershed (0.52 km^2) in southeast Wyoming. Two realistic approximations were proposed to evaluate the covariance terms of the FPE based on the statistical relationships using the topography data and the distributed fine-scale energy balance snow model (Dsnow model). The covariance of wind-caused snow redistribution was theoretically derived in terms of the variance of wind speed and land surface curvatures. Conversely, the covariance of snowmelt was evaluated using a correlation function between spatial mean and variance of snowmelt rate, obtained by analyzing the results of a distributed fine-scale snow model. Snow redistribution caused by vegetation and other factors was also considered in this method, but no physically based equation was established due to limited knowledge of these processes. A simple linear formula was introduced to express the residual effects caused by vegetation and other factors on the spatial variability of snow depth. From various model validations, the FPE model concept was considered adequate because this additional parameterization absorbed all residuals of the model simulation. More research on snow distributions using field and remote sensing observations are essential for tuning and improving of the FPE model.

In this paper, some assumptions and simplifications were introduced and implemented to evaluate the covariance terms for snow redistribution and uneven snowmelt rate. Nevertheless, the solutions of the FPE were able to reproduce the spatial variability of snow depth. The FPE approach was proven to be a promising methodology for large-scale snow process modeling when appropriate treatments of the model parameters, the atmospheric forcing, and numerical methods were selected. This modeling work, following Ohara et al. (2008), demonstrates a capability to contribute to larger-scale Earth surface modeling and to analyze coarse-resolution data gathered from remote sensing.

Before coupling this model with other land surface and hydrological models, additional model validation is desirable for transferability and scale dependency of the approximations (such as, the delta correlation approximation in the snow redistribution and the finite correlation in the snowmelt) using multiple spatial snow depth data under various climates to improve this subgrid variability snow model.

Appendix A

Derivation of equation (23).

This section provides a brief derivation of equation (23). The proportionality between friction velocity and the longitudinal variance of the wind speed in the surface layer is commonly used (Larsen & Hansen, 2014; Stull, 1988; Türk & Emeis, 2010) as

$$\sigma = \alpha \cdot u_* \tag{A1}$$

where σ is standard deviation of wind speed, u_* is mean of friction velocity, α is empirical coefficient, which is generally between 2.4 and 2.5. Using log wind profile law, the variance of friction velocity can be calculated as

$$\mathrm{var}(u_*) = \mathrm{var}\left(\frac{u\kappa}{\ln(z/z_0)}\right) = \left(\frac{\kappa}{\ln(z/z_0)}\right)^2 \mathrm{var}(u) \tag{A2}$$

where var(·) denotes a variance operator, κ is the von Karman constant (≈ 0.4), z is the measuring height, z_0 is the roughnessz length, u is mean wind speed. From equation (A1), we obtain

$$\mathrm{var}(u) = \sigma^2 = \alpha^2 u_*^2 = \alpha^2 \left(\frac{u\kappa}{\ln(z/z_0)}\right)^2 = \alpha^2 \left(\frac{\kappa}{\ln(z/z_0)}\right)^2 u^2 \tag{A3}$$

Substituting equation (A3) into (A2), we have

$$\mathrm{var}(u_*) = \alpha^2 \left(\frac{\kappa}{\ln(z/z_0)}\right)^4 u^2 \tag{A4}$$

This equation means that the variance of wind speed can be estimated from the mean wind speed during the time increment. Letting

$$m = \alpha^2 \left(\frac{\kappa}{\ln(z/z_0)}\right)^4 \tag{A5}$$

then, we have

$$\mathrm{var}(u_*) = m \cdot u^2 \tag{A6}$$

Coefficient m depends on land cover and time resolution of mean wind speed u and can be estimated from the observed high-frequency wind speed data.

Acknowledgments
We would like to thank Dr. Jeff R. Snider, the Editor Charles H. Luce, and three reviewers for providing helpful comments on the paper. We appreciate their patience in reviewing this very theoretical paper, which takes time and effort to digest. All data used in this paper are open accessed and can be downloaded through these given links: the Lidar snow depth data, https://data.uwyo.edu/islandora/object/ir%3AM2PD5Q; WRF downscale data, https://doi.org/10.15786/m2pks4; *Repeater Tower* meteorological data, https://doi.org/10.15786/m2xjqb; GPR snow depth data, https://doi.org/10.15786/m2p5db; and source code of the FPE snow model and inputs, https://doi.org/10.15786/m2x1b7. This study was supported by the National Science Foundation under award no. EPS-1208909.

References

Anderson, E. A. (1976). A point energy and mass balance model of a snow cover. Silver Spring, Md Us. National Oceanic and Atmospheric Administration (NOAA). Technical Report NWS 19.

Anderton, S. P., White, S. M., & Alvera, B. (2004). Evaluation of spatial variability in snow water equivalent for a high mountain catchment. *Hydrological Processes*, *18*(3), 435–453. https://doi.org/10.1002/hyp.1319

Avissar, R., & Pielke, R. A. (1989). A parameterization of heterogeneous land surfaces for atmospheric numerical models and its impact on regional meteorology. *Monthly Weather Review*, *117*(10), 2113–2136. https://doi.org/10.1175/1520-0493(1989)117<2113:APOHLS>2.0.CO;2

Avissar, R. (1992). Conceptual aspects of a statistical-dynamical approach to represent landscape subgrid-scale heterogeneities in atmospheric models. *Journal of Geophysical Research*, *97*(D3), 2729–2742. https://doi.org/10.1029/91JD01751

Blöschl, G. (1999). Scaling issues in snow hydrology. *Hydrological Processes*, *13*(14-15), 2149–2175. https://doi.org/10.1002/(SICI)1099-1085(199910)13:14/15<2149::AID-HYP847>3.0.CO;2-8

Bradford, J. H., Harper, J. T., & Brown, J. (2009). Complex dielectric permittivity measurements from ground-penetrating radar data to estimate snow liquid water content in the pendular regime. *Water Resources Research*, *45*, W08403. https://doi.org/10.1029/2008WR007341

Broxton, P. D., Harpold, A. A., Biederman, J. A., Troch, P. A., Molotch, N. P., & Brooks, P. D. (2015). Quantifying the effects of vegetation structure on snow accumulation and ablation in mixed-conifer forests. *Ecohydrology*, *8*(6), 1073–1094. https://doi.org/10.1002/eco.1565

Clark, M. P., Hendrikx, J., Slater, A. G., Kavetski, D., Anderson, B., Cullen, N. J., et al. (2011). Representing spatial variability of snow water equivalent in hydrologic and land-surface models: A review. *Water Resources Research*, *47*, W07539. https://doi.org/10.1029/2011WR010745

Deems, J. S., Painter, T. H., & Finnegan, D. C. (2013). Lidar measurement of snow depth: A review. *Journal of Glaciology*, *59*(215), 467–479. https://doi.org/10.3189/2013JoG12J154

DeWalle, D. R., & Rango, A. (2008). *Principles of snow hydrology*. Cambridge University Press.

Dunn, S. M., & Colohan, R. J. E. (1999). Developing the snow component of a distributed hydrological model: A step-wise approach based on multi-objective analysis. *Journal of Hydrology*, *223*(1–2), 1–16. https://doi.org/10.1016/S0022-1694(99)00095-5

Essery, R. (1997). Modelling fluxes of momentum, sensible heat and latent heat over heterogeneous snow cover. *Quarterly Journal of the Royal Meteorological Society*, *123*(543), 1867–1883. https://doi.org/10.1002/qj.49712354305

Graham, W., & McLaughlin, D. (1989). Stochastic analysis of nonstationary subsurface solute transport: 1. Unconditional moments. *Water Resources Research*, *25*(2), 215–232. https://doi.org/10.1029/WR025i002p00215

Hartman, M. D., Baron, J. S., Lammers, R. B., Cline, D. W., Band, L. E., Liston, G. E., & Tague, C. (1999). Simulations of snow distribution and hydrology in a mountain basin. *Water Resources Research*, *35*(5), 1587–1603. https://doi.org/10.1029/1998WR900096

He, S., & Ohara, N. (2017). A new formula for estimating the threshold wind speed for snow movement. *Journal of Advances in Modeling Earth Systems*, *9*, 2514–2525. https://doi.org/10.1002/2017MS000982

He, S., Ohara, N., & Miller, S. (2019). Understanding sub grid variability of snow depth at 1-km scale using Lidar measurements. *Hydrological Processes*, 1–13. https://doi.org/10.1002/hyp.13415

Heinz, S. (2011). *Mathematical modeling*, (1st ed.). Springer Publishing Company, Incorporated. https://doi.org/10.1007/978-3-642-20311-4

Heward, Jacob R. (2015). The effects of a changing landscape on snow accumulation and ablation in the Upper Little Laramie River Wyoming Watershed. Thesis, University of Wyoming.

Hirsch, C. (2007). *Numerical computation of internal and external flows: The fundamentals of computational fluid dynamics*. Butterworth-Heinemann.

Holbrook, W. S., Miller, S. N., & Provart, M. A. (2016). Estimating snow water equivalent over Long Mountain transects using snowmobile-mounted ground-penetrating radar. *Geophysics*, *81*(1), WA183–WA193. https://doi.org/10.1190/geo2015-0121.1

Horne, F. E., & Kavvas, M. L. (1997). Physics of the spatially averaged snowmelt process. *Journal of Hydrology*, *191*(1–4), 179–207. https://doi.org/10.1016/S0022-1694(96)03063-6

Isaaks, H. E., & Mohan Srivastava, R. (1989). *An introduction to applied geostatistics*, (1st ed.). New York, NY: Oxford University Press.

Kavvas, M. L. (2003). Nonlinear hydrologic processes: Conservation equations for determining their means and probability distributions. *Journal of Hydrologic Engineering*, *8*(2). American Society of Civil Engineers), 44–53. https://doi.org/10.1061/(ASCE)1084-0699(2003)8:2(44)

Kavvas, M. L., & Karakas, A. (1996). On the stochastic theory of solute transport by unsteady and steady groundwater flow in heterogeneous aquifers. *Journal of Hydrology*, *179*(1), 321–351.

Kavvas, M. L., & Wu, J. (2002). *Conservation equations for solute transport by unsteady and steady flows in heterogeneous aquifers: The cumulant expansion/lie operator method*, (pp. 281–306). VA: Stochastic Methods in Subsurface Contaminant Hydrology. ASCE Reston.

Kim, S., Kavvas, M. L., & Chen, Z. (2005). Root-water uptake model at heterogeneous soil fields. *Journal of Hydrologic Engineering*, *10*(2), 160–167. https://doi.org/10.1061/(ASCE)1084-0699(2005)10:2(160)

Kimerling, A. J., Buckley, A. R., & Muehrcke, P. C. (2012). *Map use: Reading, analysis, interpretation*. ESRI Press Academic.

Kojima, K. (1967). Densification of seasonal snow cover. *Physics of Snow and Ice: I. Conference on Physics of Snow and Ice*, *1*(2). Institute of Low Temperature Science, Hokkaido University), 929–952.

Kraus, K., & Pfeifer, N. (1998). Determination of terrain models in wooded areas with airborne laser scanner data. *ISPRS Journal of Photogrammetry and Remote Sensing*, *53*(4). Elsevier:), 193–203. https://doi.org/10.1016/S0924-2716(98)00009-4

Kure, S., Kavvas, M. L., Ohara, N., & Jang, S. (2010). Upscaling of coupled land surface process modeling for heterogeneous landscapes: Stochastic approach. *Journal of Hydrologic Engineering*, *16*(12), 1017–1029.

Larsen, G. C., & Hansen, K. S. (2014). De-trending of wind speed variance based on first-order and second-order statistical moments only. *Wind Energy*, *17*(12), 1905–1924. https://doi.org/10.1002/we.1676

Lefsky, M. A., Cohen, W. B., Parker, G. G., & Harding, D. J. (2002). Lidar remote sensing for ecosystem studies: Lidar, an emerging remote sensing technology that directly measures the three-dimensional distribution of plant canopies, can accurately estimate vegetation structural attributes and should be of particular interest to forest, landscape, and global ecologists. *Bioscience*, *52*(1), 19–30. https://doi.org/10.1641/0006-3568(2002)052[0019:LRSFES]2.0.CO;2

Liang, X., Lettenmaier, D. P., & Wood, E. F. (1996). One-dimensional statistical dynamic representation of subgrid spatial variability of precipitation in the two-layer variable infiltration capacity model. *Journal of Geophysical Research*, *101*(D16), 21403–21422. https://doi.org/10.1029/96JD01448

Liston, G. E. (1995). Local advection of momentum, heat, and moisture during the melt of patchy snow covers. *Journal of Applied Meteorology*, *34*(7), 1705–1715. https://doi.org/10.1175/1520-0450-34.7.1705

Liston, G. E. (2004). Representing subgrid snow cover heterogeneities in regional and global models. *Journal of Climate*, *17*(6), 1381–1397. https://doi.org/10.1175/1520-0442(2004)017<1381:RSSCHI>2.0.CO;2

Luce, C. H., Tarboton, D. G., & Cooley, K. R. (1998). The influence of the spatial distribution of snow on basin-averaged snowmelt. *Hydrological Processes*, *12*(10–11), 1671–1683. https://doi.org/10.1002/(SICI)1099-1085(199808/09)12:10/11<1671::AID-HYP688>3.0.CO;2-N

Luce, C. H., Tarboton, D. G., & Cooley, K. R. (1999). Sub-grid parameterization of snow distribution for an energy and mass balance snow cover model. *Hydrological Processes*, *13*(12–13), 1921–1933. https://doi.org/10.1002/(SICI)1099-1085(199909)13:12/13<1921::AID-HYP867>3.0.CO;2-S

Marchand, W.-D., Killingtveit, A., Wilén, P., & Wikstrom, P. (2003). Comparison of ground-based and airborne snow depth measurements with georadar systems, case study. *Nordic Hydrology*, *34*(5). Copenhagen: Munksgaard, 1970–2007.:), 427–448. https://doi.org/10.2166/nh.2003.0016

Menzel, L., & Lang, H. (2005). Spatial heterogeneity of snow conditions and evapotranspiration in the Swiss Alps. *Advances in Global Change Research*, 275–282. https://doi.org/10.1007/1-4020-3508-X_28

Ohara, N. (2003). *Numerical and stochastic upscaling of snowmelt process*. Dissertation: University of California, Davis.

Ohara, N. (2014). A practical formulation of snow surface diffusion by wind for watershed-scale applications. *Water Resources Research*, *50*, 5074–5089. https://doi.org/10.1002/2013WR014744

Ohara, N. (2017). An Eulerian equation for snow accumulation downstream of an object. *Water Resources Research*, *53*, 1525–1538. https://doi.org/10.1002/2016WR019673

Ohara, N., & Kavvas, M. L. (2006). Field observations and numerical model experiments for the snowmelt process at a field site. *Advances in Water Resources*, *29*(2), 194–211. https://doi.org/10.1016/j.advwatres.2005.03.016

Ohara, N., Kavvas, M. L., & Chen, Z. Q. (2008). Stochastic upscaling for snow accumulation and melt processes with PDF approach. *Journal of Hydrologic Engineering*, *13*(12), 1103–1118. https://doi.org/10.1061/(ASCE)1084-0699(2008)13:12(1103)

Reutebuch, S. E., McGaughey, R. J., Andersen, H.-E., & Carson, W. W. (2003). Accuracy of a high-resolution Lidar terrain model under a conifer forest canopy. *Canadian Journal of Remote Sensing*, *29*(5), 527–535. https://doi.org/10.5589/m03-022

Roe, P. L. (1986). Characteristic-based schemes for the Euler equations. *Annual Review of Fluid Mechanics*, *18*(1). Annual Reviews 4139 El Camino Way, PO Box 10139, Palo Alto, CA 94303–0139, USA:), 337–365. https://doi.org/10.1146/annurev.fl.18.010186.002005

Roe, P. L., & Baines, M. J. (1982). Algorithms for advection and shock problems. In *Numerical methods in fluid mechanics*, (pp. 281–290). Springer.

Seth, A., Giorgi, F., & Dickinson, R. E. (1994). Simulating fluxes from heterogeneous land surfaces: Explicit subgrid method employing the Biosphere-Atmosphere Transfer Scheme (BATS). *Journal of Geophysical Research*, *99*(18), 651–618.

Stull, R. B.1988. *An introduction to boundary layer meteorology*. Springer Science & Business Media, DOI: https://doi.org/10.1007/978-94-009-3027-8.

Sundström, Nils. (2012). Improving snow water equivalent estimates with ground penetrating radar by measuring on multiple channels. PhD thesis, Lulea University of Technology; Citeseer.

Türk, M., & Emeis, S. (2010). The dependence of offshore turbulence intensity on wind speed. *Journal of Wind Engineering and Industrial Aerodynamics*, *98*(8-9), 466–471. https://doi.org/10.1016/j.jweia.2010.02.005

Ulriksen, C., & Peter, F. (1982). Application of impulse radar to civil engineering, doctoral thesis, Dept. of Engineering Geology, Lund University of Technology, Lund, Sweden.

van Kampen, N. G. (1976). Stochastic differential equations. *Physics Reports*, *24*(3). Elsevier:), 171–228. https://doi.org/10.1016/0370-1573(76)90029-6

van Leer, B. (1974). Towards the ultimate conservative difference scheme: II. Monotonicity and conservation combined in a second-order scheme. *Journal of Computational Physics*, *14*(4). Elsevier:), 361–370. https://doi.org/10.1016/0021-9991(74)90019-9

van Leer, B. (1979). Towards the ultimate conservative difference scheme: V. Asecond-order sequel to Godunov's method. *Journal of Computational Physics*, *32*(1), 101–136. https://doi.org/10.1016/0021-9991(79)90145-1

Western, A. W., Blöschl, G., & Grayson, R. B. (1998). Geostatistical characterisation of soil moisture patterns in the Tarrawarra catchment. *Journal of Hydrology*, *205*(1-2), 20–37. https://doi.org/10.1016/S0022-1694(97)00142-X

Wetlaufer, K., Hendrikx, J., & Marshall, L. (2016). Spatial heterogeneity of snow density and its influence on snow water equivalence estimates in a large Mountainous Basin. *Hydrology*, *3*(1), 3. https://doi.org/10.3390/hydrology3010003

Wu, C.-M., Yeh, T.-C. J., Zhu, J., Lee, T. H., Hsu, N.-S., Chen, C.-H., & Sancho, A. F. (2005). Traditional analysis of aquifer tests: Comparing apples to oranges? *Water Resources Research*, *41*, W09402. https://doi.org/10.1029/2004WR003717

Yeh, P. J. F., & Eltahir, E. A. B. (2005). Representation of water table dynamics in a land surface scheme. Part II: Subgrid variability. *Journal of Climate*, *18*(12), 1881–1901. https://doi.org/10.1175/JCLI3331.1

Yoon, J., & Levent Kavvas, M. (2003). Probabilistic solution to stochastic overland flow equation. *Journal of Hydrologic Engineering*, *8*(2), 54–63. https://doi.org/10.1061/(ASCE)1084-0699(2003)8:2(54)

Zevenbergen, L. W., & Thorne, C. R. (1987). Quantitative analysis of land surface topography. *Earth Surface Processes and Landforms*, *12*(1), 47–56. https://doi.org/10.1002/esp.3290120107

Zha, Y., Yeh, T.-C. J., Shi, L., Huang, S.-Y., Wang, W., & Wen, J.-C. (2017). Quasi-steady state conditions in heterogeneous aquifers during pumping tests. *Advances in Water Resources*, *106*, 95–110. https://doi.org/10.1016/j.advwatres.2017.03.017